Earth's Future

RESEARCH ARTICLE
10.1029/2023EF004231

Projecting Global Mercury Emissions and Deposition Under the Shared Socioeconomic Pathways

Benjamin M. Geyman[1], David G. Streets[1], Colin P. Thackray[1], Christine L. Olson[2], Kevin Schaefer[2], and Elsie M. Sunderland[1,3]

[1]Harvard John A. Paulson School of Engineering and Applied Sciences, Cambridge, MA, USA, [2]National Snow and Ice Data Center, Cooperative Institute for Research in Environmental Sciences, University of Colorado Boulder, Boulder, CO, USA, [3]Department of Environmental Health, Harvard School of Public Health, Boston, MA, USA

Key Points:

- Future (2010–2300) anthropogenic Hg releases to air, land, and water (0.7–1.7 Tg) are similar to historical (1510–2010) releases (1.1–2.8 Tg)
- Cumulative future anthropogenic Hg emissions to air (2010–2300) vary by a factor of two across scenarios (110–230 Gg)
- Deposition declines from near-term reductions in anthropogenic Hg emissions are amplified by reductions in reemissions from land and the ocean

Supporting Information:

Supporting Information may be found in the online version of this article.

Correspondence to:

B. M. Geyman,
bgeyman@fas.harvard.edu

Citation:

Geyman, B. M., Streets, D. G., Thackray, C. P., Olson, C. L., Schaefer, K., & Sunderland, E. M. (2024). Projecting global mercury emissions and deposition under the shared socioeconomic pathways. *Earth's Future*, *12*, e2023EF004231. https://doi.org/10.1029/2023EF004231

Received 1 NOV 2023
Accepted 22 MAR 2024

Author Contributions:

Conceptualization: Benjamin M. Geyman, David G. Streets, Elsie M. Sunderland
Data curation: Benjamin M. Geyman, David G. Streets
Formal analysis: Benjamin M. Geyman, David G. Streets, Elsie M. Sunderland
Funding acquisition: Elsie M. Sunderland
Methodology: Benjamin M. Geyman, David G. Streets, Elsie M. Sunderland
Project administration: Elsie M. Sunderland
Software: Colin P. Thackray

Abstract Mercury (Hg) is a naturally occurring element that has been greatly enriched in the environment by human activities like mining and fossil fuel combustion. Despite commonalities in some carbon dioxide (CO_2) and Hg emission sources, the implications of long-range climate scenarios for anthropogenic Hg emissions have yet to be explored. Here, we present comprehensive projections of anthropogenic Hg emissions extending to the year 2300 and evaluate impacts on global atmospheric Hg deposition. Projections are based on four Shared Socioeconomic Pathways (SSPs) ranging from sustainable reductions in resource and energy intensity to rapid economic growth driven by abundant fossil fuel exploitation. There is a greater than two-fold difference in cumulative anthropogenic Hg emissions between the lower-bound (110 Gg) and upper-bound (235 Gg) scenarios. Hg releases to land and water are approximately six times those of direct emissions to air (600–1,470 Gg). At their peak, anthropogenic Hg emissions reach 2,200–2,600 Mg a^{-1} sometime between 2010 (baseline) and 2030, depending on the SSP scenario. Coal combustion is the largest determinant of differences in Hg emissions among scenarios. Decoupling of Hg and CO_2 emission sources occurs under low-to mid-range scenarios, though contributions from artisanal and small-scale gold mining remain uncertain. Future Hg emissions may have lower gaseous elemental Hg (Hg^0) and higher divalent Hg (Hg^{II}), resulting in a higher fraction of locally sourced Hg deposition. Projected reemissions of previously deposited anthropogenic Hg follow a similar temporal trajectory to primary emissions, amplifying the benefits of primary Hg emission reductions under the most stringent mitigation scenarios.

Plain Language Summary Mercury (Hg) is a global pollutant that is emitted alongside greenhouse gases like carbon dioxide (CO_2) when fossil fuels such as coal are burned. Researchers have projected how emissions of greenhouse gases and climate are likely to change in the future, but relatively little is known about future Hg releases. Here, we project Hg emissions between 2010 and 2300 using growth scenarios developed by the climate change research community. Under low emission scenarios, Hg emissions are projected to peak between 2010 and 2030. Under the high emission scenario, Hg releases continue near present-day levels until after 2060, and decline more slowly than other scenarios thereafter. Large variability in projected releases (cumulatively a two-fold difference) is apparent across the low and high scenarios. Globally, the intensity of coal combustion and how quickly it is phased out is the largest driver of future Hg releases. We used global models to simulate future atmospheric Hg deposition, identifying multiple factors responsible for changing deposition patterns. We find there is a penalty for delaying reductions in Hg emissions because of increased reemissions from the land and ocean in the future. This work emphasizes the benefits of stringent near-term global reductions in anthropogenic Hg releases.

1. Introduction

Mercury (Hg) is a naturally occurring element, but human activities such as mining and fossil-fuel combustion have released approximately 1.5 Tg of Hg from stable geologic reservoirs to the atmosphere, land, and water over the past 500 years (1510–2010) (Streets et al., 2019a). This has significantly altered the natural biogeochemical Hg cycle (Geyman et al., 2023; Streets et al., 2019a) and adversely affected the health of exposed humans and wildlife (Basu et al., 2023). Reemission of anthropogenic Hg from terrestrial and aquatic ecosystems extends its lifetime in the biosphere (referred to as "legacy Hg"). Past work has quantified the impacts of historical emissions and legacy Hg cycling on the global Hg cycle (Amos et al., 2013; Angot et al., 2018; Guerrero & Schneider, 2023; Nriagu, 1994). However, estimates of future anthropogenic Hg emissions based on the most recent future growth

Supervision: Elsie M. Sunderland
Visualization: Benjamin M. Geyman
Writing – original draft: Benjamin M. Geyman, David G. Streets, Elsie M. Sunderland
Writing – review & editing: Benjamin M. Geyman, David G. Streets, Colin P. Thackray, Christine L. Olson, Kevin Schaefer, Elsie M. Sunderland

scenarios adopted by the Intergovernmental Panel on Climate Change (IPCC) and their drivers are not presently available (O'Neill et al., 2016), limiting our ability to project future scenarios of Hg pollution.

Shared Socioeconomic Pathways (SSPs) and their associated emission scenarios offer unified narratives ranging from sustainable development to fossil fuel-driven growth (O'Neill et al., 2016, 2017). They provide a framework for bounding development and greenhouse gas trajectories extending to the year 2300 (Meinshausen et al., 2020). However, these narratives do not explicitly address Hg emissions or the technological transformations underpinning future changes in Hg emission intensity. We fill this gap by developing a methodology for projecting time-dependent change in activity-specific Hg emission factors. This approach is built upon detailed parameterizations developed for historical emission inventories, which facilitates intercomparison of past and future emissions (Streets et al., 2011, 2019a).

Anthropogenic Hg is released to the atmosphere in both the elemental (Hg^0) and oxidized (Hg^{II}) forms. Hg^{II} has an atmospheric lifetime against deposition of a few days (Corbitt et al., 2011), while the lifetime of Hg^0 is greater than 1 year (Horowitz et al., 2017; Shah et al., 2021). Previous studies projected Hg deposition in 2035 and 2050 based on anthropogenic Hg emissions estimated from the older IPCC Special Report on Emission Scenarios (SRES) and independent estimates (Corbitt et al., 2011; Pacyna et al., 2016; Streets et al., 2009). Results suggested that future increases in Hg^{II} emissions relative to Hg^0 are likely to increase the proportion of regional Hg deposition from emitting countries (Corbitt et al., 2011). The SRES emission trajectories ranged from a best-case scenario that showed relatively flat anthropogenic Hg emissions between 2006 and 2050, to a scenario characterized by higher energy and economic growth (A1B) that approximately doubled 2006 emission levels (Streets et al., 2009). Results from Pacyna et al. (2016) ranged from a slight increase under a current policy scenario to −85% under a maximum feasible reduction case. However, these past studies did not consider future changes in marine and terrestrial Hg reservoirs that affect reemission of Hg^0 (Amos et al., 2013, 2014). This is important because terrestrial and marine Hg^0 evasion are thought to account for large fractions of the atmospheric Hg undergoing contemporary and future deposition (e.g., ∼60% of 2050 deposition to the contiguous United States) (Corbitt et al., 2011).

The main objective of this work is to better understand how future anthropogenic Hg emissions and deposition vary among the most recent socioeconomic development pathways used by the IPCC. To do this, we developed new decadal projections of primary anthropogenic Hg emissions for the years 2010–2300 based on four distinct SSPs spanning a wide range of radiative forcings. Using a suite of global modeling tools, we quantified how changes in primary Hg emissions and reemissions from terrestrial and marine ecosystems affect regional magnitudes and global patterns in atmospheric deposition. This work provides insights into how different scenarios of fossil fuel use are likely to affect global Hg burdens and the potential effects of different pollution control efforts.

2. Methods

2.1. Description of Development Narratives (SSP Scenarios)

Forecasts of future anthropogenic Hg emissions were developed in accordance with the scenarios used in Phase 6 of the Coupled Model Intercomparison Project (CMIP6), organized under the auspices of the IPCC (O'Neill et al., 2016). The scenarios were based on a framework combining narratives of global development with emissions and climate projections from integrated assessment and climate models (O'Neill et al., 2016). The first component, the SSPs, are comprised of five distinct narratives describing alternative courses of societal development, as well as quantitative descriptions of population, economic growth, and urbanization (Dellink et al., 2017; Jiang & O'Neill, 2017; Samir & Lutz, 2017). The SSPs were elaborated using integrated assessment models (IAMs) to provide quantitative descriptions of energy use, greenhouse gas emissions, and land-use change (Riahi et al., 2017).

For each SSP narrative, multiple IAM trajectories were defined to describe both a baseline scenario, which assumes no additional climate policies or climate change impacts, and mitigation scenarios, in which further policies are adopted. SSP narratives can be combined with different climate forcing pathways to describe the physical response of the climate system. The climate forcing is defined according to the long-term global average radiative forcing (W m^{-2}; Myhre et al., 2013). Following convention, the scenarios used in this work are written as: $SSP_{x\text{-}y}$, where x is the SSP and y is the radiative forcing pathway (W m^{-2}) (O'Neill et al., 2016). Throughout the rest of this work, scenarios will be referred by their specific name (e.g., SSP1-2.6) or collectively as "SSPs."

For this work, we adopted the three major scenarios that were initially chosen for long-term extensions (LTE) to 2300 under CMIP6 (O'Neill et al., 2016), namely, SSPs 1–2.6, 5–3.4, and 5–8.5. Scenario SSP1-2.6 is a lower-bound on future emissions, reflecting strong emphasis on sustainability and intensive control of climate-forcing agents; SSP5-3.4 is known as the "*overshoot*" scenario and reflects short-term growth in fossil fuel use and minimal consideration of climate control measures until 2040 followed by aggressive mitigation thereafter; SSP5-8.5 is an upper bound emission scenario, in which fossil-fuel use continues with little consideration of climate mitigation or transition to clean technologies. Subsequently, Meinshausen et al. (2020) extended additional scenarios to beyond 2300, so we added a fourth scenario to our projections, the so-called "*middle-of-the-road*" scenario, SSP2-4.5 (Fricko et al., 2017).

The detailed raw activity data that are used in this work to characterize Hg emissions under these four scenarios out to 2100 follow the work of Riahi et al. (2017) and Rao et al. (2017), with LTE from 2100 to 2300 following the work of Meinshausen et al. (2020). The Hg emissions forecasts reported in this work map the trajectories of carbon dioxide (CO_2) forecasts contained in the previously mentioned publications and the emissions of other species, as described in subsequent studies (Gidden et al., 2019; Lund et al., 2019; Turnock et al., 2020). However, this work contains the first reported projections of Hg emissions under CMIP6 scenarios.

The SSP scenarios were used primarily to project fossil fuel use (coal and oil), the manufacture and use of refined industrial products, and economic parameters. However, there are no specific variables from which to calculate the extraction and production of raw materials and basic products because these are not directly relevant to emissions of greenhouse gases. However, they are very important as sources of mercury. Thus, for 21st century production of these materials, we used forecasts specifically generated by industry models, as follows: copper, zinc, and lead (Sverdrup et al., 2019); iron (Morfeldt et al., 2015); mercury (Sverdrup & Olafsdottir, 2020); and gold (Sverdrup et al., 2012); as well as the basic industrial products steel (Morfeldt et al., 2015) and cement (Zhang et al., 2018). The work of Watari et al. (2020, 2021) was valuable in guiding the pathways of metals extraction and use to the end of the century.

2.2. Mercury Emission Calculation

Mercury emissions under a future climate scenario (f) were calculated using Equation 1:

$$E_{t,r,s,f} = E_{2010,r,s} \times \left(\frac{A_{t,r,s,f}}{A_{2010,r,s,f}}\right) \times \left(\frac{EF_{t,r,s,f}}{EF_{2010,r,s,f}}\right), \quad (1)$$

where E = emissions (Mg a^{-1}); t = decadal future year, r = world region, s = source type; A = activity level (in various units); and EF = emission factor (g per unit of activity).

Future Hg emissions were calculated by extrapolating 2010 base year emissions, as reported in (Streets et al., 2017, 2019a), in accordance with the energy and activity forecasts for each of the four future scenarios (f) described in the previous section. Emissions were calculated for each decade between 2020 and 2300, though they reach zero between 2190 and 2250 across scenarios, in accordance with SSP prescriptions. Emissions are zero beyond 2250 across all scenarios.

Emissions were calculated at world region level (r). The SSP forecasts were developed for five world regions: OECD, REF (Russia and Eastern Europe), ASIA, MAF (Middle East and Africa), and LAM (Latin America). This is a very coarse division of the world, which may be adequate for CO_2 studies but is too aggregated for studies of Hg emissions and transport. In particular, the OECD region is spread across the globe, with contributions from Western Europe, North America (NAM), Australasia, and Japan. The prior Hg emission estimates for 2010 (Streets et al., 2019a, 2019b), upon which this work is based, were calculated for 17 world regions and subsequently aggregated to seven: NAM, South America (SAM), Western Europe (EUR), the Former Soviet Union (FSU), Africa/Middle East (AFM), Asia (ASA), and Oceania (OCA). By examining 2010 Hg emissions in the world regions used in each of these two studies, a simple equivalence was determined and applied in this work, as follows: NAM = 0.5 OECD +0.1 LAM; SAM = 0.9 LAM; EUR = 0.3 OECD; FSU = REF; AFM = MAF; ASA = ASIA +0.05 OECD; and OCA = 0.15 OECD. Emissions at the global scale (GLO) are thus identical. Though this is less than an ideal solution—because of potential future differences in the rates of development

among the countries comprising the coarse SSP regions—it is certainly an improvement over the five SSP regions from the perspective of estimating Hg transport and deposition.

The SSP scenarios contain more than 600 activity components (A), covering all aspects of future energy, industrial, and economic development. The prior 2010 Hg emission estimates were developed for 18 source types (s) (Streets et al., 2017). Because none of the SSP scenarios provide activity components that can be unequivocally associated with several of the Hg source types, emissions from 11 source types were projected individually in this work: mining (copper, zinc, lead, iron, mercury, gold, and artisanal gold), steel production, cement production, coal combustion, and oil combustion. Six other source types (municipal waste incineration, other waste combustion, electrical and measuring equipment, chemicals manufacturing, caustic soda production, and dental) were projected in aggregate. Silver mining was not included in this work because Hg emissions from 2010 onwards are expected to be zero.

The change in activity levels in the future, A_t/A_{2010}, reflects the growth or shrinkage in activity for a particular source type, in a particular region, under a particular scenario. Some may grow, some may decline, depending on the influence of the world economy in general and the pressure of the climate change scenario. For example, coal combustion may increase under a lax climate scenario or decline under a stringent one. But A_t/A_{2010} only characterizes the change in the size of the source type, it says nothing about the transformation of it over the time period in question. New, high-performing technologies will undoubtedly replace older, low-performing ones; and the imposition of new emission control regulations may or may not force the use of add-on emission control technologies or even a complete change in production technology. All of these factors will influence Hg emissions. Except for Carbon Capture and Storage and inferences from SO_2 emissions, the SSP scenarios say nothing about the technological transformations that will influence Hg emissions. This is therefore the most challenging aspect of projecting future Hg emissions. Our approach was to develop the ratio $EF_{t,r,s,f}/EF_{2010,r,s,f}$ as an indicator of how future emission rates will decline from their 2010 values. Note that this ratio is never greater than one (i.e., future emission rates are never higher in the future than in 2010 per unit of activity).

In previous work, we developed a methodology for estimating the time-development of emission factors for historical periods (pre-2010) using transformed normal distribution functions (Streets et al., 2011). These region-specific functions were parameterized based on a detailed review of experimental measurements around the world, as illustrated in that paper for copper smelting. It was shown, for example, that the Hg emission rate for copper smelters pre-1900 was an uncontrolled value of 27.5 gHg/MgCu worldwide. After 1900, emission rates declined, along different pathways in different parts of the world, reaching values in 2010 ranging from a low of 0.60 gHg/MgCu in western Europe to a high of 11.6 gHg/MgCu in Africa (Table S1 in Supporting Information S1). Regional emission factors in 2010 are shown for key processes in Tables S1 and S2 in Supporting Information S1.

The challenge in this work was to reasonably represent the continuation of historical EF trends beyond 2010 in the absence of guidance from the SSP forecasts. In this work, we focused on the period 2010–2100, where technology transformation will have the biggest effect. For each of the 11 key source types mentioned above, we assumed that by 2100 the emission rates in every world region will have declined from their 2010 levels to the present-day emission rate of the lowest-emitting region. Thus, in the case of copper smelting, all regions emit at 0.60 gHg/MgCu by 2100, though the trajectories to reach it vary by region. This 2100 rate then continues for all years beyond 2100. Intermediate years in EF were determined via linear interpolation.

For the purposes of atmospheric modeling, speciation of future atmospheric Hg emissions into elemental Hg (Hg^0) and divalent Hg (Hg^{II}) compounds was determined in a similar way, by extrapolation of the speciation splits in each region in the year 2010. As reported in previous work, Hg^0 made up about 55% of global emissions to air in 2010, with the remainder emitted as Hg^{II} (Streets et al., 2011, 2019a). These fractions vary rather widely, from a high of 88% in SAM due to extensive artisanal and small scale gold mining (ASGM) to a low of 25% in western Europe due to copper production and diffuse sources in the waste sector. The fraction of total air emissions released as Hg^0 (Hg^0/Hg ratio) is projected to decline in the future as ASGM is phased out, which emits Hg primarily as Hg^0. In this work, we assumed that the 2010 ratios in high-emitting regions approach the western European level or the North American level (33%) by 2100, eventually leveling out at a technology-limiting value of 20% everywhere. Slight variations were applied among the four scenarios to reflect anticipated patterns of future technology transformations.

Finally, future releases of Hg to land and water were estimated following the method of Streets et al. (2017, 2019a). In essence, this involves subtracting the air emissions from the total Hg contained in the raw material that is processed. It was not possible to determine *a priori* the fate of these releases by source type, technology level, or world region. Uncertainties in the few quantitative estimates that have been made and the vast quantity of unknown factors for sources in remote parts of the world essentially rule this out.

2.3. Global Atmospheric Hg Deposition

We used the GEOS-Chem global chemical transport model to simulate the atmospheric fate and deposition of Hg emissions under each SSP scenario. The model version (12.8) used here included detailed multi-phase oxidation of elemental Hg and gas-phase photolysis of oxidized Hg species from Shah et al. (2021). Simulations were run using 2014–2019 MERRA-2 meteorology (Gelaro et al., 2017) on a 2×2.5-degree horizontal grid with a 72-layer vertical domain extending through the top of the stratosphere. The first 2 years of each simulation were used for initialization and the final 3 years were averaged for analysis to reduce the effects of meteorological variability on simulated deposition patterns.

We conducted 5-year simulations for each decade from 2020 to 2100 for each scenario in addition to a common baseline scenario for the 2010 emission year. We hold meteorology constant across decadal snapshots to isolate the effects of variation in future emissions. Emissions from the seven world regions were distributed onto a 0.25×0.25-degree grid based on the spatial distributions established in prior work (Steenhuisen & Wilson, 2019). Relative fractions of North American emissions from Canada, the United States, and Central America were scaled to reflect 2015 values reported in Streets et al. (2019b) for consistency with past work.

We constructed source-receptor functions to quantify changes in atmospheric Hg deposition resulting from shifts in terrestrial and oceanic Hg^0 evasion and for each anthropogenic emission region. Following Corbitt et al. (2011), we define each source-receptor function F_{ij} as:

$$F_{ij} = \frac{D_{ij}}{E_i} \tag{2}$$

where D_{ij} is the total mercury deposition flux to receptor grid cell j from emissions in region i, and E_i is the magnitude of emissions from region i.

2.4. Global Biogeochemical Box Model (GBBM)

An updated version of the multi-compartment Global Biogeochemical Box Model (GBBM) developed by Amos et al. (2013, 2014) was used to simulate future shifts in atmospheric deposition from legacy mercury emissions (Text S1; Table S3 and S4 in Supporting Information S1). The GBBM represents Hg cycling between the atmosphere, terrestrial biosphere (fast, slow, protected), ocean (surface, intermediate, deep), and removal by burial in marine sediment.

We added four new compartments to the GBBM that represent waste reservoirs (fast, slow, protected, and immobilized) to explicitly track the fate of the estimated 1.13 Tg Hg released by humans to land and water from 1510 to 2010 (Streets et al., 2019a). These releases included tailings and waste from mining and metals production, chlor-alkali plants, and substantial contributions from Hg use in commercial products (Horowitz et al., 2014; Streets et al., 2011). In prior work, anthropogenic releases to land and water were added to soil compartments of the GBBM (Streets et al., 2017). However, it is likely that the majority of such releases are sequestered at contaminated sites and do not have the same diffuse impacts on deposition as atmospheric sources (Guerrero & Schneider, 2023; Kocman et al., 2017). Therefore, we independently tracked land and water Hg releases. We parameterized reemissions of Hg^0 and discharges of Hg^{II} to rivers from waste compartments using the same rate coefficients as for the fast, slow, and protected terrestrial Hg in the GBBM. Land and water Hg releases were partitioned into waste pools following the methods described in Streets et al. (2017) (Text S1 in Supporting Information S1).

We simulated the time-dependent fate of future anthropogenic Hg releases separately for each scenario. In each simulation, the model was initialized by calculating the steady state distribution of mercury among reservoirs under a constant geogenic Hg flux of 230 Mg a^{-1} from subaerial volcanism and 50 Mg a^{-1} from hydrothermal

10.1029/2023EF004231

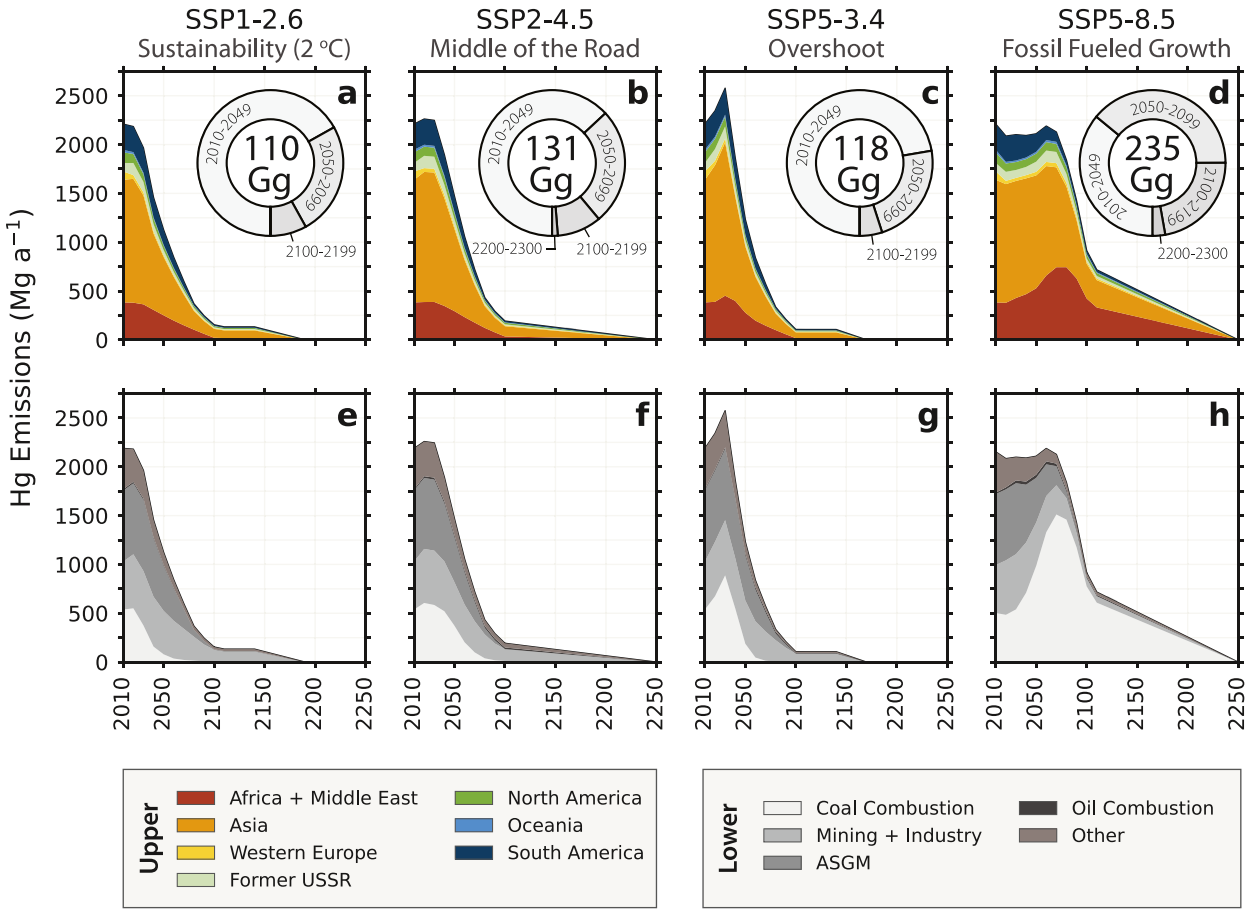

Figure 1. Global anthropogenic mercury (Hg) emissions to air by world region and source sector. Trajectories under each scenario are shown by world region in Panels (a–d). Inset pie charts show fractional emissions occurring during four "snapshot" time periods, arranged clockwise from the bottom: 2010–2049, 2050–2099, 2100–2200, 2200–2300. Cumulative emissions to air (Gg; 2010–2300) are shown in the center of each ring. Panels (e–h) provide sector-specific breakdowns of the same emissions. ASGM = artisanal and small-scale gold mining.

vents (Geyman et al., 2023). The model was forced with all-time (2000 BCE to 2010 CE) anthropogenic mercury releases from Streets et al. (2019a) followed by emissions specified in each scenario from 2010 to 2300. Evaluation of model results for the year 2010 agree with the observational ranges for the atmospheric Hg reservoir, seawater concentrations, and atmospheric deposition enrichment factors (Table S5 in Supporting Information S1, Amos et al., 2015).

3. Results and Discussion

3.1. Future Emission Trends

3.1.1. Long-Term Perspective on Anthropogenic Hg Releases

Atmospheric Hg emissions are shown by region (Figure 1; Table S6 in Supporting Information S1) and source sector (Table S7 in Supporting Information S1) for each of the four scenarios considered in this work. All primary Hg emissions are projected to be zero beyond 2250, consistent with SSP assumptions. Projected cumulative Hg releases to air, land, and water between 2010 and 2300 range from 709 Gg under SSP1-2.6, to 1,710 Gg under SSP5-8.5. Projected anthropogenic emissions between 2010 and 2300 are comparable to cumulative historical emissions from 1510 to 2010 (1,470 Gg) estimated in past work (Streets et al., 2019a), suggesting human impacts on the global Hg cycle will be sustained for millennia.

Global Hg emissions projected in this work for the year 2050 are substantially lower than similar forecasts made over a decade prior (2300–4,900 Mg a^{-1}) using the IPCC SRES scenarios (Streets et al., 2009). The projected

decrease in emissions in 2050 under SSP1-2.6 (−1,080 Mg a^{-1}) is similar to that projected for 2035 by Pacyna et al. (2016) under a scenario involving full implementation of policy commitments and plans made before 2016. Relative declines projected in this work are partially attributable to lower Hg emission factors from recently implemented Hg pollution controls (e.g., Zhang et al., 2023). Thus, lower future Hg emissions estimated in this work reflect progress made through global policy efforts in recent decades.

Across all scenarios, future land and water Hg releases follow qualitatively similar trajectories to atmospheric emissions. Land and water releases grow as a fraction of total anthropogenic releases in the future. By 2100, anthropogenic Hg releases to land and water are estimated to be 12 to 25 times greater than anthropogenic Hg emissions to air, compared to only 3.3-fold greater (7,330 Mg a^{-1}) in 2010.

3.1.2. Scenario-Specific Patterns in Primary Anthropogenic Hg Releases

Among scenarios considered in this work, SSP1-2.6 is a lower-bound greenhouse gas emissions case, and it is known as the "2 °C scenario." SSP1-2.6 is characterized by aggressive reductions in greenhouse gas emissions and a nameplate end-of-century radiative forcing of 2.6 W m^{-2} (Meinshausen et al., 2020). Projected future atmospheric Hg emissions decline continuously after 2010 (Figures 1a and 1e). In 2010, Asia was the largest regional contributor (1,260 Mg a^{-1}; 57% of total) to global atmospheric emissions (2210 Mg a^{-1}). Under SSP1-2.6, a 93% reduction in global Hg emissions is projected (154 Mg a^{-1}) by the year 2100, and Asia remains the largest remaining regional emitter (91 Mg a^{-1}, 59%). Beyond 2100, emissions continue to decline at a slower pace and reach zero by 2190, in accordance with SSP assumptions.

SSP2-4.5 is a middle-of-the-road scenario that reflects moderate socioeconomic, energy, and climate mitigation changes and a continuation of growth and development trajectories following the status quo (Meinshausen et al., 2020). Relative to 2010, Hg emissions grow slightly until 2030 and then decline at a rate similar to SSP1-2.6 (Figures 1b and 1f). Hg emissions are 193 Mg a^{-1} by 2100, which is only 25% greater than SSP1-2.6 (Figures 1b and 1f). SSP2-4.5 is not nearly as close to the "middle of the road" for Hg emissions as it is for carbon emissions because it relies heavily on a switch from coal to natural gas as the primary energy supply under moderate climate mitigation efforts. This strategy results in continued greenhouse gas emissions and middle-of-the-road climate effects, but much lower Hg emissions because natural gas releases insignificant quantities of Hg. Hg emissions under SSP2-4.5 continue at a low level into the distant future, eventually reaching zero in 2250 following SSP assumptions (Figures 1b and 1f). Between 2010 and 2300, cumulative emissions to air are 131 Gg and cumulative emissions to land and water are 737 Gg under SSP2-4.5.

SSP5-3.4 is the "overshoot" case characterized by a delay in climate-change action until after 2030, leading to a major rise in Hg emissions between 2010 and 2030. Hg emissions are projected to rise to 2,580 Mg a^{-1} by 2030, an increase of 17% over 2010 (Figures 1c and 1g). Much of that growth occurs in Asia. After 2030, emissions decline more precipitously than under the other three scenarios, reaching levels similar to SSP1-2.6 by 2060. Hg emissions fall to 107 Mg a^{-1} by 2100 and reach zero in the year 2170, which is earlier than under SSP1-2.6. Under SSP5-3.4, cumulative emissions to air are projected to be 118 Gg. Compared to SSP1-2.6, cumulative emissions are heavily weighted toward the first few decades of the projection period. Cumulative emissions to land and water are 618 Gg.

SSP5-8.5 is the upper-bound case, characterized by continued fossil fuel use and minimal consideration of environmental sustainability. Under this scenario, CO_2 concentrations are projected to reach levels greater than 2,000 ppm by 2200 (Meinshausen et al., 2020). Such levels have not occurred on Earth since before the onset of the modern Antarctic glaciation over 40 Mya (Rae et al., 2021), and are associated with temperatures 3.3°C–5.7°C higher in 2100 than during the early industrial period (1850–1900) (IPCC, 2023). Emissions of Hg to air remain near present levels until after 2060 and then decline to 914 Mg a^{-1} (5–9 times the other scenarios) by the end of the 21st century. The dominant Hg emission regions are Asia, where emissions exceed 1,000 Mg a^{-1} through 2070, and Africa and the Middle East, where emissions grow from 383 Mg a^{-1} in 2010 to 744 Mg a^{-1} in 2080. Emissions decline slowly beyond 2100, remaining at high levels into the 22nd century: 512 Mg a^{-1} in 2150 and 256 Mg a^{-1} in 2200 (Figures 1d and 1h). Emissions do not reach zero until 2250. Cumulative Hg releases (2010–2300) are 235 Gg to air and 1.47 Tg to land and water under SSP5-8.5.

Several indicators suggest that global anthropogenic Hg emissions may be tracking below levels described in the overshoot scenario (SSP5-3.4) since 2010. While growth in anthropogenic Hg emissions between 2010 and 2015

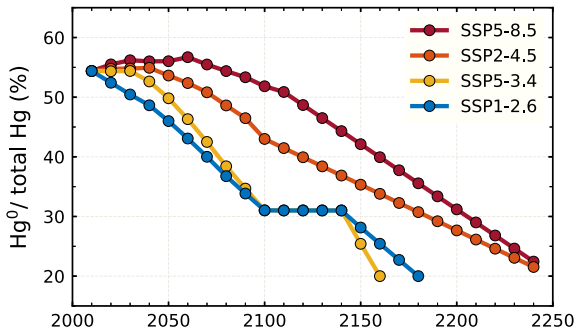

Figure 2. Decadal changes in the speciation of primary anthropogenic mercury (Hg) emissions to air. The percentage of total Hg emissions to air released as elemental Hg (Hg^0) is shown for each scenario and the remaining fraction consists of divalent mercury (Hg^{II}).

exceeds SSP-based projections from 2010–2020 (Streets et al., 2019b; Figure S1 in Supporting Information S1), domestic policies have resulted in widespread installation of air pollution control devices over the past decade in China (Zhang et al., 2023) and the United States (Dai et al., 2023). Trends in Hg^0 concentrations and isotopic composition from long-term monitoring sites in China also show declines consistent with reductions in regional anthropogenic emissions (Wu et al., 2023). Such trends in other developing and industrializing parts of the world remain to be confirmed.

3.1.3. Decoupling of Hg Emissions and Radiative Forcing Under Low Coal-Use Scenarios

Among source sectors in 2010, artisanal ASGM was the largest global source of atmospheric emissions (727 Mg a^{-1}), followed by coal combustion (538 Mg a^{-1}) and mining and industry (491 Mg a^{-1}) (Table S6 in Supporting Information S1). Large-scale (rather than ASGM) gold production was the largest source of Hg released to land and water (1,990 Mg a^{-1}), followed by ASGM (1,090 Mg a^{-1}), electrical and measurement equipment (1,010 Mg a^{-1}), chemicals manufacturing (860 Mg a^{-1}), and zinc smelting (670 Mg a^{-1}). Coal combustion accounted for a greater fraction of global atmospheric emissions (25%) in 2010 compared to land and water releases (5%, 370 Mg a^{-1}).

Differences in future anthropogenic Hg emissions to air principally reflect differences in coal combustion across SSP scenarios. Hg emissions from coal combustion are projected to grow by 2.3%–12.5% and peak in 2020 under SSPs 1–2.6 and 2–4.5 (Figures 1e and 1f). Near-term increases in Hg emissions from coal combustion reach levels 65% higher than 2010 under SSP5-3.4. Hg emissions decline thereafter for lower coal-use scenarios (SSPs 1–2.6, 2–4.5, and 5–3.4; Figures 1e–1g). By 2050, they fall to a fraction of 2010 levels (15% under SSP1-2.6% and 69% under SSP2-4.5) and reach zero before the end of the century. In contrast, coal combustion persists until 2250 under SSP5-8.5. Coal-related Hg emissions under SSP5-8.5 reach 990 Mg a^{-1} (96% higher than 2010) by 2070 and remain 44% higher than 2010 levels by the end of the century (Figure 1h).

Among lower coal-use scenarios, coal combustion is responsible for 16 Gg (SSP1-2.6) to 28 Gg (SSP2-4.5) of cumulative (2010–2300) Hg emissions to air. Cumulative Hg emissions to air from coal combustion are ∼5 to 9-fold greater under SSP5-8.5 (139 Gg) than the other scenarios, and coal combustion comprises 59% of all emissions to air between 2010 and 2300 under SSP5-8.5.

Despite relative similarities in the phase-out of coal, SSPs 1–2.6, 2–4.5, and 5–3.4 show very different greenhouse gas emission trajectories. Such differences arise from rates of natural gas and oil combustion, as well as carbon capture and sequestration. These factors exert minimal direct influence on primary anthropogenic Hg emissions, though they produce disparate climate effects. For example, end-of-century surface temperatures simulated with the NASA GISS-E2.1 climate model are 1.8°C–2.3°C higher than the preindustrial (1850–1880) mean under SSP1-2.6 compared to 2.7°C–3.3°C under SSP2-4.5 (Nazarenko et al., 2022). The degree of warming will modulate future changes in Hg emissions from the natural biosphere (e.g., Krabbenhoft & Sunderland, 2013; Schaefer et al., 2020). Therefore, it is important to consider the consequences of human activity for both direct anthropogenic Hg releases and warming-driven changes in Hg cycling in the biosphere and ocean (e.g., Schaefer et al., 2020; Schartup et al., 2019).

3.1.4. Changes in Hg Emission Speciation Favor Local and Regional Deposition

The fraction of primary anthropogenic Hg emissions released to air as Hg^0 is projected to decline in the future (Figure 2), with implications for transboundary pollution. For SSP1-2.6, the fraction of Hg^0 emitted by primary sources is projected to decline by 23% between 2010 and 2100. It stabilizes from 2100 to 2140, and then declines continuously thereafter. By 2180, the last decade with non-zero emissions for SSP1-2.6, Hg^0 is projected to make up just 20% of total anthropogenic Hg emissions to air (Figure 2). Emission speciation under SSP5-3.4 broadly follows that of SSP1-2.6, with slightly higher Hg^0 fractions until 2100, and an accelerated decline between 2140 and 2160 from 31% Hg^0 to 20% Hg^0 (Figure 2). Under SSP2-4.5, Hg^0 comprises a larger fraction of total Hg emissions to air than under SSPs 1–2.6 and 5–3.4, remaining around 55% until 2040 (Figure 2). The Hg^0 fraction then exhibits a slow decline with overall emissions and reaches 22% by 2240 (Figure 2). SSP5-8.5 consistently

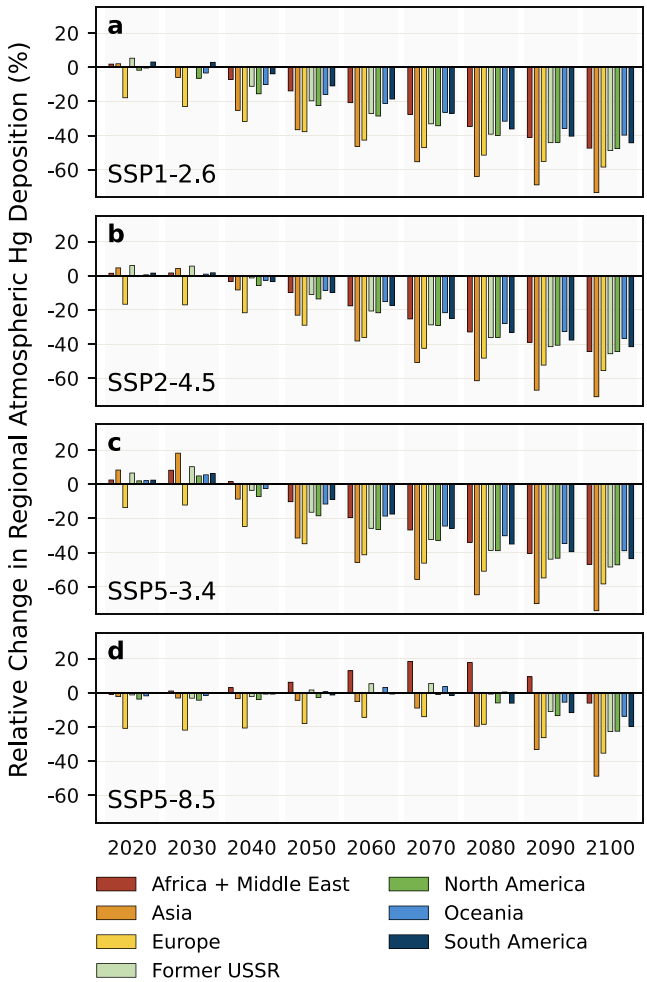

Figure 3. Relative changes in regional atmospheric mercury (Hg) deposition compared to 2010. Changes in atmospheric Hg deposition are shown by world region (represented by colored bars) for each decade from 2020 to 2100 (*x*-axis). Each subplot represents temporal trends under a different Shared Socioeconomic Pathway (SSP) scenario (O'Neill et al., 2016).

represents an upper bound for the Hg^0 fraction, increasing to 57% in 2060, followed by near-continuous declines to reach 22% by 2240. While trajectories vary across scenarios, greater fractions of Hg^{II} relative to Hg^0 in primary anthropogenic emissions are expected to produce future deposition patterns from primary emissions that increasingly reflect local and regional rather than global sources (Figure S2 in Supporting Information S1).

3.2. Future Deposition Patterns From Primary Anthropogenic Emissions

Modeled global Hg deposition to land increases by 22 Mg a^{-1} (0.9%) between 2010 and 2020 under SSP1-2.6 emissions. This reflects increases from both primary anthropogenic emissions (+8 Mg a^{-1}) and higher reemissions from terrestrial and ocean surfaces due to increasing Hg reservoirs (+14 Mg a^{-1}) (Figure S3 in Supporting Information S1). Modeled increases in regional Hg deposition occur during this period over all global regions except for Europe and North America (Figure 3a; Figure 4a). There, declines in deposition from primary anthropogenic sources exceed increases in deposition from growing global terrestrial and oceanic Hg reservoirs and subsequent reemissions. From 2040 through the end of the century, declines in atmospheric Hg deposition are projected for all regions. By 2100, total atmospheric Hg deposition is projected to be less than half of 2010 levels (46%, 1,120 Mg a^{-1}) (Figure S3 in Supporting Information S1). The largest regional deposition declines are projected over Asia (−510 Mg a^{-1}; −73%) because it was the largest source region in 2010 (Figure 3a).

Temporal patterns in atmospheric Hg deposition under SSP2-4.5 are qualitatively similar to those of SSP1-2.6, characterized by slight but regionally heterogeneous near-term increases that give way to continuous decreases. Relative to 2010, global deposition increases by 1.7% in 2020 and 1.6% in 2030. These increases occur over all regions except Europe, where declines are smaller than for SSP1-2.6 (−17% in 2020 and 2030) (Figure 3b). By the end of the century, deposition to land is 1,270 Mg a^{-1} lower than in 2010 (Figure S3 in Supporting Information S1), with regional declines reaching 71% (−25 μg m^{-2} a^{-1}) in Asia (Figure 3b).

Under SSP5-3.4, near-term deposition increases considerably, growing to 2,690 Mg a^{-1} (+9%) in 2030 over land (Figure S3 in Supporting Information S1). The greatest increases occur in Asia, where total Hg deposition reaches 41 μg m^{-2} a^{-1} (+18%) in 2030. Deposition grows by greater than 8% over all regions except Europe. After 2030, accelerated emission reductions relative to SSP1-2.6 result in comparable end-of-century deposition, which is 1,340 Mg a^{-1} lower than in 2010 (Figure S3 in Supporting Information S1).

Atmospheric deposition under SSP5-8.5 is much higher than the other scenarios through most of the century. However, 2020 deposition is the lowest of all scenarios, and 2030 deposition is lower than all scenarios other than SSP1-2.6 (Figure S3 in Supporting Information S1). Growth in emissions from Africa and the Middle East, combined with sustained emissions elsewhere, produce increasing deposition over most regions from 2020 until 2070. Most notably, deposition to Africa and the Middle East reach levels 18% higher (+2.5 μg m^{-2} a^{-1}) by 2070 and remain above baseline levels through 2100 (Figure 3d; Figure S3 in Supporting Information S1). End-of-century total deposition to land is 650 Mg a^{-1} lower than in 2010.

3.3. Implications for Legacy Hg Deposition From Terrestrial and Aquatic Emissions

Scenarios for deposition of legacy Hg vary among the four SSPs. Legacy deposition peaks before 2035 at levels 20–62 Mg a^{-1} higher than 2010 under SSPs 1–2.6, 2–4.5, and 5–3.4 (Figure 5). Legacy deposition under SSP5-8.5 exhibits a larger and later peak, exceeding 2010 deposition by 66 Mg a^{-1} in 2071 (Figure 5). By 2100, relative trends in legacy deposition are notably different, with declines of 330–380 Mg a^{-1} relative to 2010 for

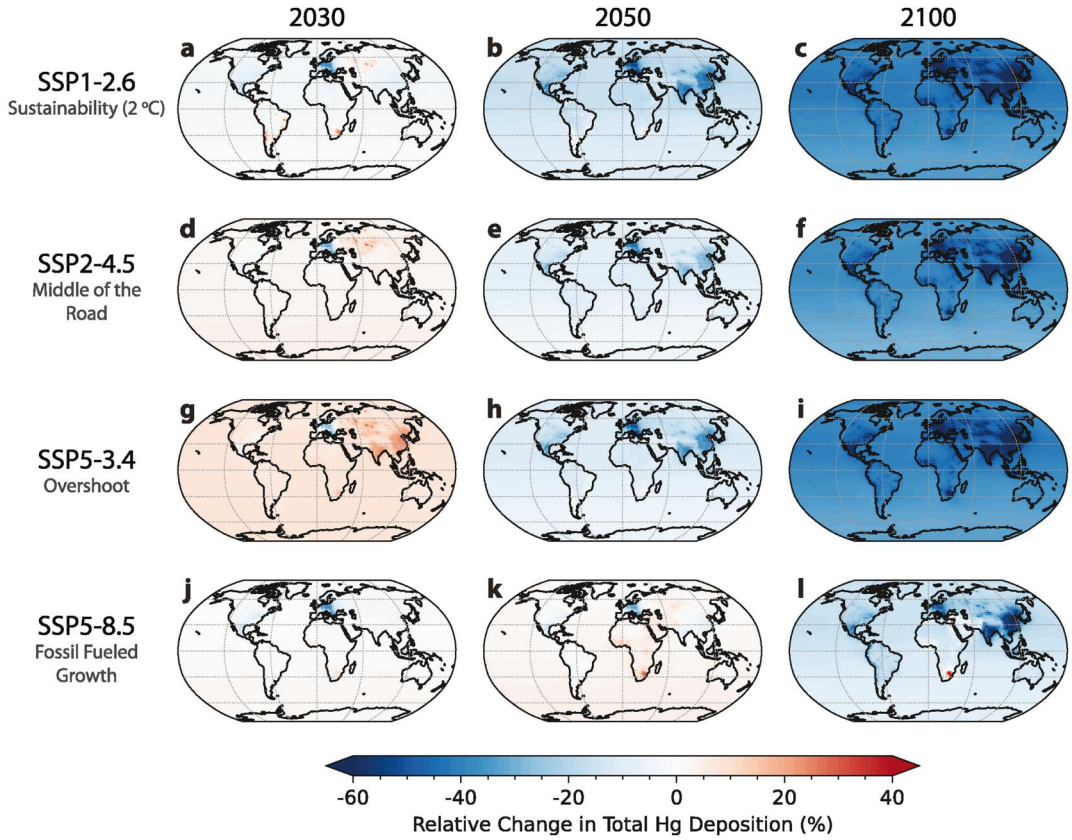

Figure 4. Trajectories of global atmospheric mercury (Hg) deposition. Panels represent fractional change in total deposition relative to the 2010 baseline by scenario (rows) for three time periods: 2030 (left column), 2050 (center column) and 2100 (right column). Deposition is calculated as the sum of deposition from primary, legacy, and natural Hg emissions using the GEOS-Chem atmospheric mercury model (Shah et al., 2021) and the Global Biogeochemical Box Model (GBBM; Amos et al., 2013, 2014).

SSPs 1–2.6, 2–4.5 and 5–3.4, compared with a decline of 47 Mg a^{-1} for SSP5-8.5 (Figure 5). These end-of-century declines in legacy emissions are responsible for 26%–28% of total declines in atmospheric Hg deposition to land under SSPs 1–2.6, 2–4.5, and 5–3.4, compared to 7% for SSP5-8.5.

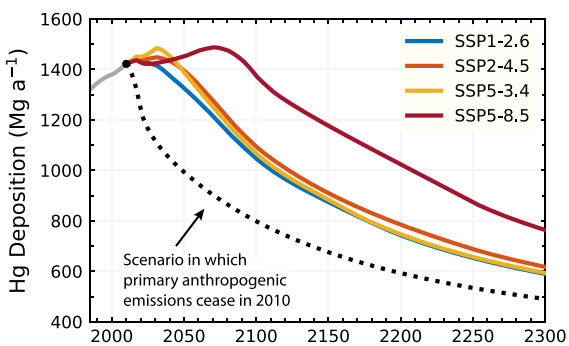

Figure 5. Mercury (Hg) deposition to land from legacy and natural emissions. Trajectories under future emissions (2010–2300) are shown for Shared Socioeconomic Pathways 1–2.6 (blue line), 2–4.5 (orange line), 5–3.4 (yellow line), and 5–8.5 (red line), in addition to a hypothetical scenario where primary anthropogenic emissions are zero after 2010 (dotted black line). Implications of future trajectories for upper ocean reservoirs are shown in Figure S4 in Supporting Information S1.

Comparing SSPs 1–2.6 and 5–3.4 provides insights into the consequences of delaying emission reductions. Cumulative emissions through 2100 are comparable for SSP1-2.6 (101 Gg) and SSP5-3.4 (112 Gg). Additionally, anthropogenic Hg emissions are lower in 2100 under SSP5-3.4 than SSP1-2.6 (107 Mg a^{-1} and 154 Mg a^{-1}). Higher deposition to anthropogenic receptor regions in 2100 under SSP5-3.4 reflects a legacy deposition penalty for the unrestrained growth of the first three decades of the century. Deposition from legacy emissions is 20 Mg higher in 2100 for SSP5-3.4 compared to SSP1-2.6, whereas deposition from primary anthropogenic emissions is 16 Mg lower. This example demonstrates the long-term benefits associated with near-term emissions mitigation, as discussed previously in Angot et al. (2018) and Amos et al. (2013).

By the end of the century, Hg reemissions from the ocean and land will become relatively more important as sources of Hg deposition (Figure S4 in Supporting Information S1), but deposition will not be evenly distributed by world region. Our source-receptor modeling suggests that South America receives the largest share of legacy Hg deposition on a per-area basis, receiving 23% higher deposition per unit of terrestrial emissions and 48%

10.1029/2023EF004231

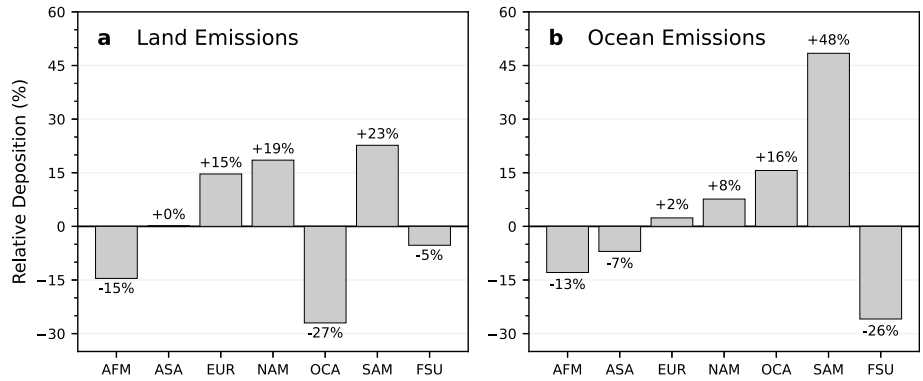

Figure 6. Regional differences in area-normalized atmospheric Hg deposition from natural and legacy sources. Bars represent differences in areal deposition rates between individual receptor regions and the average over land. Positive values mean that receptor regions receive greater deposition per unit area than average, and negative values mean that receptor regions receive less deposition than average. Individual panels show trends in deposition resulting from emissions from the terrestrial biosphere (a) and from the ocean (b). Receptor regions are Africa and the Middle East (AFM), Asia (ASA), Europe (EUR), North America, Oceania (OCA), South America, and the Former Soviet Union.

higher deposition per unit of ocean evasion than the area-weighted average of all world regions (Figure 6). Such high rates of deposition over South America are driven by high rates of foliar uptake and wet deposition. In contrast, Oceania receives the lowest areal share of terrestrial emissions (73% of average), and the Former USSR receives the smallest areal share of Hg sourced from oceanic evasion (74% of average) (Figure 6). Such low deposition is driven by the relative isolation of Oceania from terrestrial emissions and of the Former USSR from ocean emissions. These source-receptor relationships are subject to change in the future due to shifting patterns of historical anthropogenic Hg loading (e.g., Zolkos et al., 2022) and changing biogeochemical dynamics mediating deposition (e.g., Alexander & Mickley, 2015; Krabbenhoft & Sunderland, 2013; Yang et al., 2019).

Globally averaged seawater Hg concentrations in the upper ocean (0–1,500 m) are projected to increase over the coming decades across all scenarios in this study. The Hg reservoir in the upper ocean peaks at 142–151 Gg between 2037 (SSP1-2.6) and 2081 (SSP5-8.5) (Figure S5 in Supporting Information S1). Near-term increases in upper ocean Hg concentrations are driven by future rather than historical emissions. Simulated seawater Hg concentrations begin declining in 2015 under a scenario with no future primary anthropogenic Hg releases (Figure S5 in Supporting Information S1). By the end of the 21st century, upper ocean Hg concentrations are projected to be 15% lower than 2010 under SSP1-2.6 and are 11% higher than 2010 under SSP5-8.5.

3.4. Limitations

Scenario-based projections are a valuable tool for exploring plausible pathways of future change under an internally coherent set of variables (O'Neill et al., 2020). However, projections are only valid within the scope of their assumptions and quantitative drivers. The Hg emission projections provided in this work extend the SSPs to quantify changes in the activity levels and emission factors of Hg-producing processes. Adapting the SSPs for projection of certain processes such as metals production necessitated mapping independent industry forecasts onto each scenario, which may reduce degrees of differentiation in emissions between scenarios for such categories. Additionally, as inconsistencies inevitably develop between quantitative SSP drivers and future conditions, it may be useful to periodically update associated Hg projections as recommended by O'Neill et al. (2020) for all projections utilizing the SSP framework. Periodic updates may be particularly important for projections of Hg speciation in air emissions, which are largely driven in this work based on regional differences in 2010 and projections about shifts in the mixture of Hg-producing sectors. However, development and adoption of Hg control technologies will likely cause significant impacts to emission speciation in categories such as coal combustion, where existing techniques such as flue-gas desulphurization, fabric filters, and electrostatic precipitators effectively remove Hg^{II}, and where developing technologies such as sorbent injection may target Hg^{0} emissions (Srivastava et al., 2006; G. Zhang et al., 2019).

Given the uncertainties inherent in long-term projection, a rationale for the multi-century projection timeframe used here is important to explain. Many components of the global Hg cycle are sensitive to present human actions

over timescales ranging from decades to centuries (Amos et al., 2013). Release of Hg from permafrost, for example, will occur over centuries (Schaefer et al., 2020). Permafrost Hg release will be largely mediated by changes to the thermal state of permafrost soils, with the process of thaw lagging the changing radiative balance of the atmosphere, which in turn lags greenhouse gas emissions. While much of the Hg which will be released from permafrost soils has been stored there for millennia, it is plausible given the dominant role of humans in the contemporary global Hg cycle that the magnitude of Hg released from permafrost may depend in part on present and future Hg deposition to permafrost regions. In this case and others, it may be useful to pair the future Hg emission and deposition trajectories presented in this work with process-based assessments of the impacts of global change on Hg biogeochemistry.

Finally, we reiterate that the changes in legacy Hg emissions and deposition presented in this work are solely functions of the anthropogenic Hg forcing and observed properties of the contemporary global Hg cycle. Fluxes of Hg are changing in response to warming in a complex and interacting manner across the Earth system, which will affect rates of legacy emissions and deposition (Sonke et al., 2023). At present, we feel there is not enough comprehensive understanding of the mechanisms driving changes in Hg cycling to justify the adoption of time-varying (non-first-order) rates in mass balance modeling. However, this is a useful focus for future research that may strive to incorporate the effects of both warming and primary Hg emissions on changing global Hg cycling.

4. Conclusions

The SSP scenarios evaluated in this work result in a greater than two-fold difference in cumulative anthropogenic Hg emissions between 2010 and 2300. Cumulative anthropogenic emissions to air and releases to land and water between 2010 and 2300 range from 710 Gg under the low-bound scenario (SSP1-2.6) to 1,710 Gg under the upper-bound scenario (SSP5-8.5). These future releases are comparable to all-time historical anthropogenic emissions prior to 2010 of 1,540 Gg (80% CI: 1,060–2,800 Gg) (Streets et al., 2019a).

Transition of the energy sector away from coal combustion is the largest determinant of differences among scenarios, with lower-bound and mid-range scenarios (SSPs 1–2.6, 2–4.5, 5–3.4) all exhibiting similar cumulative emissions due to declining coal usage. By contrast, industrial Hg mining and ASGM releases are projected to grow in relative importance in the future. These results imply that under the most stringent climate policies, the largest sources of Hg and CO_2 are likely to become more distinct from one another.

Numerous factors may affect regional Hg deposition patterns in the future. For most regions, reducing primary anthropogenic Hg emissions remains the most effective way to reduce deposition, since 55%–71% of Hg^{II} emissions redeposit to the region of origin, compared to 5%–13% for Hg^0 (Figure S6 in Supporting Information S1). However, the scenario-based trajectories described in this work indicate that anthropogenic Hg^{II} emissions to air will decline more slowly than Hg^0, causing Hg^{II} to grow as a fraction of total anthropogenic Hg emissions to air. As the speciation of anthropogenic Hg emissions shifts toward lower fractions of Hg^0, a greater proportion of regional emissions will redeposit to the region of origin. Across all regions, the fraction of atmospheric Hg deposition that originates from emissions within the same regions is projected to increase from 33% in 2010 to 35%–45% in 2100 (Figure S2 in Supporting Information S1).

Regional atmospheric Hg deposition patterns over the next century reflect trends in the magnitude and spatial distribution of primary anthropogenic emissions as well as reemissions from the land and ocean. In regions where anthropogenic Hg emission reductions are projected to occur, total Hg deposition is expected to decrease, even during periods where global deposition is increasing. This means that domestic policies have significant leverage on domestic Hg deposition (e.g., Dai et al., 2023). However, greater reductions in anthropogenic emissions are accompanied by larger declines in emissions from the land and ocean. Under SSP1-2.6, 28% of the reduction in atmospheric deposition from 2010 to 2100 is the result of declines in legacy emissions. As a result, globally coordinated efforts to reduce near-term anthropogenic Hg emissions will produce amplified benefits in terms of long-term declines in atmospheric deposition (e.g., Angot et al., 2018).

Data Availability Statement

Mercury emission files, model output, and supporting data are available on the Harvard Dataverse (Geyman, 2024). Reproduction code (Geyman & Thackray, 2024) and the GEOS-Chem v12.8.0 model (The

International GEOS-Chem User Community, 2020) are archived on Zenodo. Activity components are from the International Institute for Applied Systems Analysis (IIASA) SSP Database (2018 release; version 2.0), available at https://tntcat.iiasa.ac.at/SspDb/. Activity components are from the AIM/CGE model for SSPs 1–2.6 and 2–4.5, from GCAM4 for SSP5-3.4, and from REMIND-MAgPIE for SSP5-8.5.

Acknowledgments
Financial support for this work was provided by the U.S. National Science Foundation (award numbers 2210173 and 2108452). The authors declare no competing financial interest. We thank Zig Klimont of International Institute for Applied Systems Analysis (IIASA) for providing the detailed activity and emissions data sets for the SSPs used in this work. The computations in this paper were run on the FASRC Cannon cluster supported by the FAS Division of Science Research Computing Group at Harvard University.

References

Alexander, B., & Mickley, L. J. (2015). Paleo-perspectives on potential future changes in the oxidative capacity of the atmosphere due to climate change and anthropogenic emissions. *Current Pollution Reports*, *1*(2), 57–69. https://doi.org/10.1007/s40726-015-0006-0

Amos, H. M., Jacob, D. J., Kocman, D., Horowitz, H. M., Zhang, Y., Dutkiewicz, S., et al. (2014). Global biogeochemical implications of mercury discharges from rivers and sediment burial. *Environmental Science & Technology*, *48*(16), 9514–9522. https://doi.org/10.1021/es502134t

Amos, H. M., Jacob, D. J., Streets, D. G., & Sunderland, E. M. (2013). Legacy impacts of all-time anthropogenic emissions on the global mercury cycle. *Global Biogeochemical Cycles*, *27*(2), 410–421. https://doi.org/10.1002/gbc.20040

Amos, H. M., Sonke, J. E., Obrist, D., Robins, N., Hagan, N., Horowitz, H. M., et al. (2015). Observational and modeling constraints on global anthropogenic enrichment of mercury. *Environmental Science & Technology*, *49*(7), 4036–4047. https://doi.org/10.1021/es5058665

Angot, H., Hoffman, N., Giang, A., Thackray, C. P., Hendricks, A. N., Urban, N. R., & Selin, N. E. (2018). Global and local impacts of delayed mercury mitigation efforts. *Environmental Science and Technology*, *52*(22), 12968–12977. https://doi.org/10.1021/acs.est.8b04542

Basu, N., Bastiansz, A., Dórea, J. G., Fujimura, M., Horvat, M., Shroff, E., et al. (2023). Our evolved understanding of the human health risks of mercury. *Ambio*, *52*(5), 877–896. https://doi.org/10.1007/s13280-023-01831-6

Corbitt, E. S., Jacob, D. J., Holmes, C. D., Streets, D. G., & Sunderland, E. M. (2011). Global source-receptor relationships for mercury deposition under present-day and 2050 emissions scenarios. *Environmental Science and Technology*, *45*(24), 10477–10484. https://doi.org/10.1021/es202496y

Dai, M. Q., Geyman, B. M., Hu, X. C., Thackray, C. P., & Sunderland, E. M. (2023). Sociodemographic disparities in mercury exposure from United States coal-fired power plants. *Environmental Science and Technology Letters*, *10*(7), 589–595. https://doi.org/10.1021/acs.estlett.3c00216

Dellink, R., Chateau, J., Lanzi, E., & Magné, B. (2017). Long-term economic growth projections in the Shared Socioeconomic Pathways. *Global Environmental Change*, *42*, 200–214. https://doi.org/10.1016/j.gloenvcha.2015.06.004

Fricko, O., Havlik, P., Rogelj, J., Klimont, Z., Gusti, M., Johnson, N., et al. (2017). The marker quantification of the Shared Socioeconomic Pathway 2: A middle-of-the-road scenario for the 21st century. *Global Environmental Change*, *42*, 251–267. https://doi.org/10.1016/j.gloenvcha.2016.06.004

Gelaro, R., McCarty, W., Suárez, M. J., Todling, R., Molod, A., Takacs, L., et al. (2017). The modern-era retrospective analysis for research and applications, version 2 (MERRA-2). *Journal of Climate*, *30*(14), 5419–5454. https://doi.org/10.1175/JCLI-D-16-0758.1

Geyman, B. M. (2024). Replication data for: Projecting global mercury emissions and deposition under the shared socioeconomic pathways [Dataset]. *Harvard Dataverse*, *V2*. https://doi.org/10.7910/DVN/UIEZW5

Geyman, B. M., & Thackray, C. P. (2024). SunderlandLab/future-hg-ssps: Publication release (v1.1) [Software]. *Zenodo*. https://doi.org/10.5281/zenodo.10672520

Geyman, B. M., Thackray, C. P., Jacob, D. J., & Sunderland, E. M. (2023). Impacts of volcanic emissions on the global biogeochemical mercury cycle: Insights from satellite observations and chemical transport modeling. *Geophysical Research Letters*, *50*(21), e2023GRL104667. https://doi.org/10.1029/2023GL104667

Gidden, M. J., Riahi, K., Smith, S. J., Fujimori, S., Luderer, G., Kriegler, E., et al. (2019). Global emissions pathways under different socio-economic scenarios for use in CMIP6: A dataset of harmonized emissions trajectories through the end of the century. *Geoscientific Model Development*, *12*(4), 1443–1475. https://doi.org/10.5194/gmd-12-1443-2019

Guerrero, S., & Schneider, L. (2023). The global roots of pre-1900 legacy mercury. *Proceedings of the National Academy of Sciences*, *120*(31), e2304059120. https://doi.org/10.1073/pnas.2304059120

Horowitz, H. M., Jacob, D. J., Amos, H. M., Streets, D. G., & Sunderland, E. M. (2014). Historical mercury releases from commercial products: Global environmental implications. *Environmental Science & Technology*, *48*(17), 10242–10250. https://doi.org/10.1021/es501337j

Horowitz, H. M., Jacob, D. J., Zhang, Y., Dibble, T. S., Slemr, F., Amos, H. M., et al. (2017). A new mechanism for atmospheric mercury redox chemistry: Implications for the global mercury budget. *Atmospheric Chemistry and Physics*, *17*(10), 6353–6371. https://doi.org/10.5194/acp-17-6353-2017

Intergovernmental Panel on Climate Change (IPCC). (2023). Summary for policymakers. In *Climate change 2021 – The physical science basis: Working Group I contribution to the sixth assessment Report of the intergovernmental panel on climate change* (pp. 3–32). Cambridge University Press. https://doi.org/10.1017/9781009157896.001

Jiang, L., & O'Neill, B. C. (2017). Global urbanization projections for the shared socioeconomic pathways. *Global Environmental Change*, *42*, 193–199. https://doi.org/10.1016/j.gloenvcha.2015.03.008

Kocman, D., Wilson, S., Amos, H., Telmer, K., Steenhuisen, F., Sunderland, E., et al. (2017). Toward an assessment of the global inventory of present-day mercury releases to freshwater environments. *International Journal of Environmental Research and Public Health*, *14*(2), 138. https://doi.org/10.3390/ijerph14020138

Krabbenhoft, D. P., & Sunderland, E. M. (2013). Global change and mercury. *Science*, *341*(6153), 1457–1458. https://doi.org/10.1126/science.1242838

Lund, M. T., Myhre, G., & Samset, B. H. (2019). Anthropogenic aerosol forcing under the shared socioeconomic pathways. *Atmospheric Chemistry and Physics*, *19*(22), 13827–13839. https://doi.org/10.5194/acp-19-13827-2019

Meinshausen, M., Nicholls, Z. R. J., Lewis, J., Gidden, M. J., Vogel, E., Freund, M., et al. (2020). The shared socio-economic pathway (SSP) greenhouse gas concentrations and their extensions to 2500. *Geoscientific Model Development*, *13*(8), 3571–3605. https://doi.org/10.5194/gmd-13-3571-2020

Morfeldt, J., Nijs, W., & Silveira, S. (2015). The impact of climate targets on future steel production – An analysis based on a global energy system model. *Journal of Cleaner Production*, *103*, 469–482. https://doi.org/10.1016/j.jclepro.2014.04.045

Myhre, G., Shindell, D., Bréon, F.-M., Collins, W., Fuglestvedt, J., Huang, J., et al. (2013). Anthropogenic and natural radiative forcing. In T. F. Stocker, D. Qin, G.-K. Plattner, M. Tignor, S. K. Allen, J. Boschung, et al. (Eds.), *Climate change 2013: The physical science Basis. Contribution of working Group I to the fifth assessment Report of the intergovernmental panel on climate change*. Cambridge University Press.

Nazarenko, L. S., Tausnev, N., Russell, G. L., Rind, D., Miller, R. L., Schmidt, G. A., et al. (2022). Future climate change under SSP emission scenarios with GISS-E2.1. *Journal of Advances in Modeling Earth Systems*, *14*(7), e2021MS002871. https://doi.org/10.1029/2021MS002871

Nriagu, J. O. (1994). Mercury pollution from the past mining of gold and silver in the Americas. *Science of the Total Environment*, *149*(3), 167–181. https://doi.org/10.1016/0048-9697(94)90177-5

O'Neill, B. C., Carter, T. R., Ebi, K., Harrison, P. A., Kemp-Benedict, E., Kok, K., et al. (2020). Achievements and needs for the climate change scenario framework. *Nature Climate Change*, *10*(12), 1074–1084. https://doi.org/10.1038/s41558-020-00952-0

O'Neill, B. C., Kriegler, E., Ebi, K. L., Kemp-Benedict, E., Riahi, K., Rothman, D. S., et al. (2017). The roads ahead: Narratives for shared socioeconomic pathways describing world futures in the 21st century. *Global Environmental Change*, *42*, 169–180. https://doi.org/10.1016/j.gloenvcha.2015.01.004

O'Neill, B. C., Tebaldi, C., van Vuuren, D. P., Eyring, V., Friedlingstein, P., Hurtt, G., et al. (2016). The scenario model intercomparison project (ScenarioMIP) for CMIP6. *Geoscientific Model Development*, *9*(9), 3461–3482. https://doi.org/10.5194/gmd-9-3461-2016

Pacyna, J. M., Travnikov, O., Simone, F. D., Hedgecock, I. M., Sundseth, K., Pacyna, E. G., et al. (2016). Current and future levels of mercury atmospheric pollution on a global scale. *Atmospheric Chemistry and Physics*, *16*(19), 12495–12511. https://doi.org/10.5194/acp-16-12495-2016

Rae, J. W. B., Zhang, Y. G., Liu, X., Foster, G. L., Stoll, H. M., & Whiteford, R. D. M. (2021). Atmospheric CO_2 over the past 66 million years from marine archives. *Annual Review of Earth and Planetary Sciences*, *49*(1), 609–641. https://doi.org/10.1146/annurev-earth-082420-063026

Rao, S., Klimont, Z., Smith, S. J., Van Dingenen, R., Dentener, F., Bouwman, L., et al. (2017). Future air pollution in the shared socio-economic pathways. *Global Environmental Change*, *42*, 346–358. https://doi.org/10.1016/j.gloenvcha.2016.05.012

Riahi, K., van Vuuren, D. P., Kriegler, E., Edmonds, J., O'Neill, B. C., Fujimori, S., et al. (2017). The Shared Socioeconomic Pathways and their energy, land use, and greenhouse gas emissions implications: An overview. *Global Environmental Change*, *42*, 153–168. https://doi.org/10.1016/j.gloenvcha.2016.05.009

Samir, K. C., & Lutz, W. (2017). The human core of the shared socioeconomic pathways: Population scenarios by age, sex and level of education for all countries to 2100. *Global Environmental Change*, *42*, 181–192. https://doi.org/10.1016/j.gloenvcha.2014.06.004

Schaefer, K., Elshorbany, Y., Jafarov, E., Schuster, P. F., Striegl, R. G., Wickland, K. P., & Sunderland, E. M. (2020). Potential impacts of mercury released from thawing permafrost. *Nature Communications*, *11*(1), 4650. https://doi.org/10.1038/s41467-020-18398-5

Schartup, A. T., Thackray, C. P., Qureshi, A., Dassuncao, C., Gillespie, K., Hanke, A., & Sunderland, E. M. (2019). Climate change and overfishing increase neurotoxicant in marine predators. *Nature*, *572*(7771), 648–650. https://doi.org/10.1038/s41586-019-1468-9

Shah, V., Jacob, D. J., Thackray, C. P., Wang, X., Sunderland, E. M., Dibble, T. S., et al. (2021). Improved mechanistic model of the atmospheric redox chemistry of mercury. *Environmental Science & Technology*, *55*(21), 14445–14456. https://doi.org/10.1021/acs.est.1c03160

Sonke, J. E., Angot, H., Zhang, Y., Poulain, A., Björn, E., & Schartup, A. (2023). Global change effects on biogeochemical mercury cycling. *Ambio*, *52*(5), 853–876. https://doi.org/10.1007/s13280-023-01855-y

Srivastava, R. K., Hutson, N., Martin, B., Princiotta, F., & Staudt, J. (2006). Control of mercury emissions from coal-fired electric utility boilers. *Environmental Science & Technology*, *40*(5), 1385–1393. https://doi.org/10.1021/es062639u

Steenhuisen, F., & Wilson, S. J. (2019). Development and application of an updated geospatial distribution model for gridding 2015 global mercury emissions. *Atmospheric Environment*, *211*(December 2018), 138–150. https://doi.org/10.1016/j.atmosenv.2019.05.003

Streets, D. G., Devane, M. K., Lu, Z., Bond, T. C., Sunderland, E. M., & Jacob, D. J. (2011). All-time releases of mercury to the atmosphere from human activities. *Environmental Science and Technology*, *45*(24), 10485–10491. https://doi.org/10.1021/es202765m

Streets, D. G., Horowitz, H. M., Jacob, D. J., Lu, Z., Levin, L., ter Schure, A. F. H., & Sunderland, E. M. (2017). Total mercury released to the environment by human activities. *Environmental Science & Technology*, *51*(11), 5969–5977. https://doi.org/10.1021/acs.est.7b00451

Streets, D. G., Horowitz, H. M., Lu, Z., Levin, L., Thackray, C. P., & Sunderland, E. M. (2019a). Five hundred years of anthropogenic mercury: Spatial and temporal release profiles. *Environmental Research Letters*, *14*(8), 084004. https://doi.org/10.1088/1748-9326/ab281f

Streets, D. G., Horowitz, H. M., Lu, Z., Levin, L., Thackray, C. P., & Sunderland, E. M. (2019b). Global and regional trends in mercury emissions and concentrations, 2010–2015. *Atmospheric Environment*, *201*(December 2018), 417–427. https://doi.org/10.1016/j.atmosenv.2018.12.031

Streets, D. G., Zhang, Q., & Wu, Y. (2009). Projections of global mercury emissions in 2050. *Environmental Science and Technology*, *43*(8), 2983–2988. https://doi.org/10.1021/es802474j

Sverdrup, H., Koca, D., & Granath, C. (2012). Modelling the gold market, explaining the past and assessing the physical and economical sustainability of future scenarios. In *Proceedings of the 30th international conference of the system dynamics society* (pp. 1–23).

Sverdrup, H. U., & Olafsdottir, A. H. (2020). System dynamics modelling of the global extraction, supply, price, reserves, resources and environmental losses of mercury. *Water, Air, and Soil Pollution*, *231*(8), 1–22. https://doi.org/10.1007/s11270-020-04757-x

Sverdrup, H. U., Olafsdottir, A. H., & Ragnarsdottir, K. V. (2019). On the long-term sustainability of copper, zinc and lead supply, using a system dynamics model. *Resources, Conservation and Recycling X*, *4*, 100007. https://doi.org/10.1016/j.rcrx.2019.100007

The International GEOS-Chem User Community. (2020). geoschem/geos-chem: GEOS-Chem 12.8.0 (v12.8.0) [Software]. *Zenodo*. https://doi.org/10.5281/zenodo.3784796

Turnock, S. T., Allen, R. J., Andrews, M., Bauer, S. E., Deushi, M., Emmons, L., et al. (2020). Historical and future changes in air pollutants from CMIP6 models. *Atmospheric Chemistry and Physics*, *20*(23), 14547–14579. https://doi.org/10.5194/acp-20-14547-2020

Watari, T., Nansai, K., Giurco, D., Nakajima, K., McLellan, B., & Helbig, C. (2020). Global metal use targets in line with climate goals. *Environmental Science & Technology*, *54*(19), 12476–12483. https://doi.org/10.1021/acs.est.0c02471

Watari, T., Nansai, K., & Nakajima, K. (2021). Major metals demand, supply, and environmental impacts to 2100: A critical review. *Resources, Conservation and Recycling*, *164*, 105107. https://doi.org/10.1016/j.resconrec.2020.105107

Wu, X., Fu, X., Zhang, H., Tang, K., Wang, X., Zhang, H., et al. (2023). Changes in atmospheric gaseous elemental mercury concentrations and isotopic compositions at Mt. Changbai during 2015–2021 and Mt. Ailao during 2017–2021 in China. *Journal of Geophysical Research: Atmospheres*, *128*(10), e2022JD037749. https://doi.org/10.1029/2022JD037749

Yang, Y., Meng, L., Yanai, R. D., Montesdeoca, M., Templer, P. H., Asbjornsen, H., et al. (2019). Climate change may alter mercury fluxes in northern hardwood forests. *Biogeochemistry*, *146*(1), 1–16. https://doi.org/10.1007/s10533-019-00605-1

Zhang, C. Y., Han, R., Yu, B., & Wei, Y. M. (2018). Accounting process-related CO2 emissions from global cement production under Shared Socioeconomic Pathways. *Journal of Cleaner Production*, *184*, 451–465. https://doi.org/10.1016/j.jclepro.2018.02.284

Zhang, G., Wang, Z., Cui, L., Zhang, X., Chen, S., & Dong, Y. (2019). Efficient removal of elemental mercury from coal-fired flue gas over sulfur-containing sorbent at low temperatures. *ACS Omega*, *4*(21), 19399–19407. https://doi.org/10.1021/acsomega.9b02825

Zhang, Y., Zhang, L., Cao, S., Liu, X., Jin, J., & Zhao, Y. (2023). Improved anthropogenic mercury emission inventories for China from 1980 to 2020: Toward more accurate effectiveness evaluation for the Minamata convention. *Environmental Science & Technology*, *57*(23), 8660–8670. https://doi.org/10.1021/acs.est.3c01065

Zolkos, S., Zhulidov, A. V., Gurtovaya, T. Y., Gordeev, V. V., Berdnikov, S., Pavlova, N., et al. (2022). Multidecadal declines in particulate mercury and sediment export from Russian rivers in the pan-Arctic basin. *Proceedings of the National Academy of Sciences*, *119*(14). https://doi.org/10.1073/pnas.2119857119

References From the Supporting Information

Bai, X., Tian, H., Zhu, C., Luo, L., Hao, Y., Liu, S., et al. (2023). Present knowledge and future perspectives of atmospheric emission inventories of toxic trace elements: A critical review. *Environmental Science & Technology*, *57*(4), 1551–1567. https://doi.org/10.1021/acs.est.2c07147

Ballabio, C., Jiskra, M., Osterwalder, S., Borrelli, P., Montanarella, L., & Panagos, P. (2021). A spatial assessment of mercury content in the European Union topsoil. *Science of the Total Environment*, *769*, 144755. https://doi.org/10.1016/j.scitotenv.2020.144755

Cui, X., Lamborg, C. H., Hammerschmidt, C. R., Xiang, Y., & Lam, P. J. (2021). The effect of particle composition and concentration on the partitioning coefficient for mercury in three ocean basins. *Frontiers in Environmental Chemistry*, *2*(May), 1–16. https://doi.org/10.3389/fenvc.2021.660267

Fitzgerald, W. F., Engstrom, D. R., Lamborg, C. H., Tseng, C. M., Balcom, P. H., & Hammerschmidt, C. R. (2005). Modern and historic atmospheric mercury fluxes in northern Alaska: Global sources and arctic depletion. *Environmental Science and Technology*, *39*(2), 557–568. https://doi.org/10.1021/es049128x

Hararuk, O., Obrist, D., & Luo, Y. (2013). Modelling the sensitivity of soil mercury storage to climate-induced changes in soil carbon pools. *Biogeosciences*, *10*(4), 2393–2407. https://doi.org/10.5194/bg-10-2393-2013

Holmes, C. D., Jacob, D. J., Corbitt, E. S., Mao, J., Yang, X., Talbot, R., & Slemr, F. (2010). Global atmospheric model for mercury including oxidation by bromine atoms. *Atmospheric Chemistry and Physics*, *10*(24), 12037–12057. https://doi.org/10.5194/acp-10-12037-2010

Lamborg, C. H., Von Damm, K. L., Fitzgerald, W. F., Hammerschmidt, C. R., & Zierenberg, R. (2006). Mercury and monomethylmercury in fluids from Sea Cliff submarine hydrothermal field, Gorda Ridge. *Geophysical Research Letters*, *33*(17), L17606. https://doi.org/10.1029/2006GL026321

Lamborg, C. H., Hammerschmidt, C. R., Bowman, K. L., Swarr, G. J., Munson, K. M., Ohnemus, D. C., et al. (2014). A global ocean inventory of anthropogenic mercury based on water column measurements. *Nature*, *512*(7512), 65–68. https://doi.org/10.1038/nature13563

Lamborg, C. H., Hammerschmidt, C. R., & Bowman, K. L. (2016). An examination of the role of particles in oceanic mercury cycling. *Philosophical Transactions of the Royal Society A: Mathematical, Physical & Engineering Sciences*, *374*(2081), 20150297. https://doi.org/10.1098/rsta.2015.0297

Li, C., Sonke, J. E., Le Roux, G., Piotrowska, N., Van der Putten, N., Roberts, S. J., et al. (2020). Unequal anthropogenic enrichment of mercury in Earth's northern and southern hemispheres. *ACS Earth and Space Chemistry*, *4*(11), 2073–2081. https://doi.org/10.1021/acsearthspacechem.0c00220

Obrist, D. (2012). Mercury distribution across 14 U.S. Forests. Part II: Patterns of methyl mercury concentrations and areal mass of total and methyl mercury. *Environmental Science & Technology*, *46*(11), 5921–5930. https://doi.org/10.1021/es2045579

Obrist, D., Pokharel, A. K., & Moore, C. (2014). Vertical profile measurements of soil air suggest immobilization of gaseous elemental mercury in mineral soil. *Environmental Science & Technology*, *48*(4), 2242–2252. https://doi.org/10.1021/es4048297

Olson, C. I., Geyman, B. M., Thackray, C. P., Krabbenhoft, D. P., Tate, M. T., Sunderland, E. M., & Driscoll, C. T. (2022). Mercury in soils of the conterminous United States: Patterns and pools. *Environmental Research Letters*, *17*(7), 074030. https://doi.org/10.1088/1748-9326/ac79c2

Smith-Downey, N. V., Sunderland, E. M., & Jacob, D. J. (2010). Anthropogenic impacts on global storage and emissions of mercury from terrestrial soils: Insights from a new global model. *Journal of Geophysical Research*, *115*(G3), G03008. https://doi.org/10.1029/2009JG001124

Soerensen, A. L., Sunderland, E. M., Holmes, C. D., Jacob, D. J., Yantosca, R. M., Skov, H., et al. (2010). An improved global model for air-sea exchange of mercury: High concentrations over the North Atlantic. *Environmental Science & Technology*, *44*(22), 8574–8580. https://doi.org/10.1021/es102032g

Sunderland, E. M., & Mason, R. P. (2007). Human impacts on open ocean mercury concentrations. *Global Biogeochemical Cycles*, *21*(4). https://doi.org/10.1029/2006GB002876

UN Environment. (2019). *Global mercury assessment 2018* (p. 62). UN Environment Programme, Chemicals and Health Branch.

UNEP. (2013). *Global Mercury Assessment 2013: Sources, emissions, releases, and environmental transport*. UNEP Chemicals Branch. Retrieved from https://wedocs.unep.org/20.500.11822/7984

Zhang, Y., Jacob, D. J., Dutkiewicz, S., Amos, H. M., Long, M. S., & Sunderland, E. M. (2015). Biogeochemical drivers of the fate of riverine mercury discharged to the global and Arctic oceans. *Global Biogeochemical Cycles*, *29*(6), 854–864. https://doi.org/10.1002/2015GB005124